The 2010 IEEE/RSJ International Conference on
Intelligent Robots and Systems
October 18-22, 2010, Taipei, Taiwan

# Design of a Variable Impedance Differential Actuator for Wearable Robotics Applications

Nevio Luigi Tagliamonte, Fabrizio Sergi, Giorgio Carpino, Dino Accoto and Eugenio Guglielmelli

*Abstract*— **In the design of wearable robots, the possibility of dynamically regulating the mechanical output impedance is crucial to achieve an efficient and safe human-robot interaction and to produce useful emergent dynamical behaviors.**

**In this paper we propose a Variable Impedance Differential Actuator (VIDA) for wearable robotics applications. The system comprises two actuators (one being an impedance-controlled rotary Series Elastic Actuator) connected through a Harmonic Drive in a differential configuration used to separately control output position and mechanical impedance. Design choices regarding the overall architecture and the single components are presented and discussed. The mechanical structure also comprises a custom-made torsion spring designed after a CAD/FEM optimization. An electromechanical model of the system has been developed and a control strategy, based on the equilibrium point approach, is simulated to validate the performances of the system against system requirements.**

**The actuation architecture allows to implement a control strategy where an equilibrium position and impedance field are simultaneously and independently regulated. This is possible still adopting very simple control laws: two controls for position and impedance regulation of the two input shafts.**

## I. INTRODUCTION

To obtain a safe human-robot interaction the stiff actuation paradigm has been substituted by the concepts of compliance and adaptability [1], [2]. In the field of wearable robotics for performance augmentation or functional restoring, robots do not rigidly move the limbs of a subject through a prescribed pattern, but they offer assistance as needed or interacts with the human producing emergent dynamical behaviors.

Robots compliance can be either achieved by actively controlling stiff actuators to mimic visco-elastic characteristics, or by directly employing passive elastic elements (also with variable mechanical properties).

The first example of a compliant actuator employing a passive elastic element is the Series Elastic Actuator (SEA) reported in [3], in which a spring is connected in series between the actuator and the load to obtain an intrinsic low output impedance across the frequency spectrum. Force control can be implemented using as feedback signal the measurement of the elastic element deflection. This approach provides the possibility of storing energy and attenuating impact shocks. A number of (rotary) prototypes of SEAs have been developed in recent years for human-robot interaction purposes (e.g. [4], [5], [6]).

Many redundant actuation architectures have developed to independently control position and stiffness; some of them may comprise stiff actuators connected in series, as in [7] or in [8], where a planetary gear train allows the serial connection. Other developments exploit the advantages of passive elastic elements to regulate output stiffness. Four main approaches have been identified in [9]: *equilibrium controlled stiffness* [3]; *antagonistic controlled stiffness* [10], [11]; *structure controlled stiffness* [12], [13]; *mechanically controlled stiffness* [14], [15].

The Variable Stiffness Actuator (VSA) was presented in [16]; in this unit three pulleys are connected by a belt which is tensioned by three springs. Two pulleys are controlled by servo motors, and allow an antagonistic configuration; non linearity of the first two springs is provided by the tensioning mechanism. The third spring has the function of keeping the belt in contact with the first two pulleys. An improvement of this prototype (VSA-II) has been presented in [17]. In [13] a Variable Stiffness Joint (VSJ) for a robot manipulator is presented; the stiffness is provided by leaf springs, whose effective length can be varied, and two actuators are used to control the position and stiffness of the joint. The position is controlled by rotating the two actuators at the same speed in the same direction; the stiffness is controlled when the two actuators rotate with different speed. The VS-Joint (Variable Stiffness Joint) presented in [15] is composed of two motors of different size to separately regulate link position and joint stiffness. A Harmonic Drive gear is used in a differential mode: a high power motor for the regulation of the position is connected to the Wave Generator, a Variable Stiffness Mechanism (VSM) is connected to the Circular Spline and the output link is connected to the Flexible Spline. The VSM is composed of four spiral springs whose linear deflection is transformed by a cam-based system in a centering torque against the compliant joint deflection. A small and light motor regulates the springs preload to change the resultant joint stiffness.

### A. Objectives

The authors are developing a novel non-anthropomorphic wearable robot for gait assistance using a design methodology where both robot morphology and control are co-evolved in a simulation environment to optimize the dynamical interaction with the human body. The design methodology under investigation is expected to boost robot "embodied intelligence", which has been demonstrated as fundamental in legged locomotion of biological and artificial agents [18]. Since the system must properly respond and adapt to the impedance patterns of human walking, actuation modules with tunable dynamical properties have to be integrated. To

All the authors are with the Laboratory of Biomedical Robotics and Biomicrosystems, Faculty of Biomedical Engineering, Università Campus Bio-Medico di Roma, Via Álvaro del Portillo, 21 - 00128 Roma, Italy.
Corresponding author: n.tagliamonte@unicampus.it

cope with this necessity a new actuation module, capable of producing variable impedance fields, is being designed.

*1) Design requirements:* Since the main application of the VIDA is wearable robotics, the major design objective is reducing size and weight. It is reasonable to require the actuator to have a weight less than 2 kg and to be contained in a volume of $150\times100\times100$ mm$^3$. The actuator should be able to generate a maximum instantaneous torque of 30 N·m and a continuous torque of 15 N·m (to assist walking with about the 30% of the physiological lower limbs joints torques). The low-force control bandwidth should be around 10 Hz and the resolution of torque measurement should be at least 0.1 N·m. The minimal impedance of the actuator should be as low as possible, so to allow a transparent behavior if needed. Since it is important to respond to high-frequency shocks deriving from the interaction with the ground, an intrinsically compliant element should be included in the architecture. Actuators presented in section I only implement variable stiffness; in our case, also a variable damping is required. Moreover impedance has do be changed with time constants comparable to motion, in order to cope with swing/stance phases of walking. VIDA design, including the overview of the architecture, a description of the control and expected performances, is presented in the following sections.

## II. DESIGN

The VIDA has a redundant actuation, with one motor (Position Regulator, PR) used to regulate the position and the second one (Impedance Regulator, IR) to modulate the mechanical impedance (considering the joint as a second order system, stiffness and damping values can be varied). The two actuators are connected to a Harmonic Drive in differential mode. A scheme of the VIDA architecture and a comparison with SEA architecture is reported in Fig. 1. In the VIDA system the series elastic element is substituted by a software controlled variable impedance implemented through the IR.

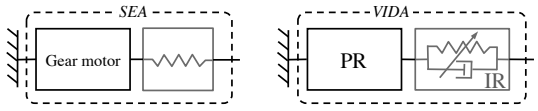


Fig. 1. Architectures of SEA (left) and VIDA (right).

The possibility of directly modulating the intrinsic visco-elastic properties of mechanical elements would result in a more energy-efficient variable impedance actuator. Anyway, a system including *structure controlled* [9] spring and damper elements would be very complex and heavy. For this reason virtual impedance is chosen to be rendered via an active software control. Moreover, this choice also allows to have a quick and flexible impedance regulation.

In the following paragraphs the design of the different components of the architecture will be separately described.

### A. Harmonic Drive gearing

In the proposed VIDA architecture the Harmonic Drive operates as a differential gearing to allow a serial connection of the two motors; in particular, the Wave Generator (WG) and the Circular Spline (CS) are the inputs and the Flexible Spline (FS) is the output. The equivalent impedance seen from the output (in our case the FS) is:

$$Z_{out} = \frac{Z_{CS} Z_{WG} N^2}{(N+1)^2 Z_{WG} + Z_{CS}}. \quad (1)$$

For high values of the transmission ratio $N$, $Z_{out} \approx Z_{CS}$. On the basis of this consideration, the IR is connected to the CS while the PR is connected to the WG (which has high transmission ratio with respect to the FS shaft) to get a rigid behavior. The selected gearing is the CSD-20-160-2A-GR, which has a transmission ratio $N = 160$, a weight of 130 g and a thickness of 14 mm.

### B. Position Regulator - PR

Many manufacturers of electrical motors include flat DC motors in their catalogues, which show to be a good compromise between high torque/power and low volume/mass.

A flat motor is used as Position Regulator: Maxon EC45-flat, 50 W brushless DC motor (251601) with a maximum continuous torque of 84.3 mN·m, a stall torque of 822 mN·m and weight of 110 g. This motor is equipped with a Maxon HEDL5540 Encoder, which has a resolution of 0.18 deg.

### C. Impedance Regulator - IR

The Impedance Regulator tunes the impedance field around the equilibrium position set by PR. A low level torque control is needed to implement an impedance control. An ideal torque generator would be desirable; to this aim a rotary SEA is used. The main advantage of series elasticity is the possibility of increasing the torque control loop gain (still maintaining desired stability margins) thus allowing a low output impedance, tolerance to shock loading, robustness to changing loads, reduction of the effects of internal stiction, friction and backlash [19]. Moreover, at frequencies above the closed-loop bandwidth the output impedance reduces to the stiffness of the series elastic element. For the IR the same motor and encoder as for the PR are used, with an additional reduction gear. To minimize the longitudinal encumbrance a (second) Harmonic Drive, equal to the one presented in section II-A, has been chosen.

*1) Passive elastic element:* The selection of the spring stiffness emerges as a tradeoff between the large force bandwidth and a low intrinsic impedance: the definition of an operational bandwidth for which the actuator needs to display large forces places a lower bound, while the upper bound is set by the need of minimizing the intrinsic impedance [19]. In our case a stiffness of 200 N·m/rad has been selected.

Several solutions have been adopted to implement a torsion elastic element. In [15] a cam-based system transforms the linear deflection of four spiral springs in a centering torque against the compliant joint deflection. In [5] six linear

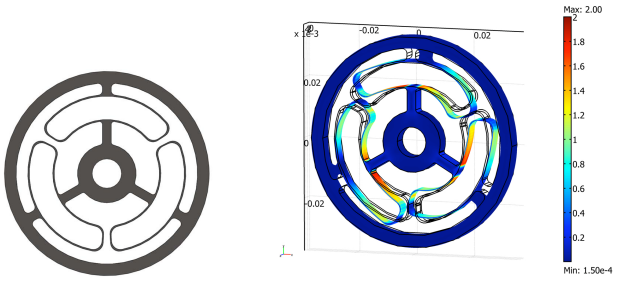


(a) (b)

Fig. 2. (a): Front view of the optimized torsion spring (the outer ring has an external diameter of 70 mm; the inner ring has an internal diameter of 10 mm; the overall thickness is 5 mm). (b): FEM analysis of the optimized torsion spring. Deformed shape (1:1 scale) and von Mises stress (GPa) are reported for the loading condition of a 30 N·m torque applied on the outer ring.

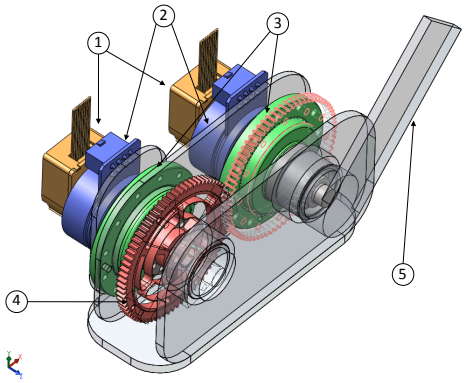


Fig. 3. 3D CAD drawing of the VIDA system. 1: encoders, 2: flat motors, 3: HD gears, 4: custom torsion spring, 5: output link. PR components are on the right side, IR components are on the left. Motion is transmitted through a 1:1 transmission ratio gear connecting the the series elastic element to the CS of the differential HD. The case is shown in transparency, with overall dimensions of 150×85×100 mm (along the $x$, $y$ and $z$ axes, respectively).

springs with a three-spoke shaft are used; in [21] a similar approach is followed with 4 springs.

In order to have a lightweight and thin torsion spring we designed a compliant disc opportunely shaped (Fig. 2a). The spring is made of maraging steel (type 18Ni, alloy 350, yield stress of 2.4 GPa) and it has an external diameter of 70 mm and a thickness of 5 mm. A FEM analysis has been performed to optimize the shape in order to achieve the desired stiffness. With reference to Fig. 2b a 30 N·m torque is applied on the outer ring (maximum instantaneous torque of the VIDA system), while the inner ring is fixed. Under these conditions a rotation of 8.6 deg is achieved, demonstrating the desired stiffness of 200 N·m/rad.

*2) Torque measurements:* The stiffness of the spring also influences the resolution of torque measurement. A 15 bit magnetic encoder (sensor PMIS4 and magnetic wheel PMIR4, ASM) is placed on the FS of the differential HD so to measure the deflection of the torsion spring (by difference with the angular position of the IR motor). This choice permits to directly monitor the output shaft of the whole actuator and to estimate the torque applied by the IR with a resolution of 0.038 N·m.

### *D. Overall mechanical structure*

In Fig. 3 a 3D CAD drawing of the VIDA system is shown. The overall architecture includes two flat motors and relative encoders, two HD gears (one used in differential configuration and the other one used as a reduction gear), an encoder on the output shaft, the custom torsion spring, a 1:1 transmission ratio gear to transmit spring rotation to the CS of the differential HD.

## III. MODEL AND CONTROL

A block diagram of the whole system, comprising the HD, the IR and the PR, is reported in Fig. 4.

### *A. Harmonic Drive model*

Modeling of Harmonic Drives in their most usual configurations has widely been investigated; the case of no fixed shaft (differential gearing configuration) has been analyzed in [20]. The kinematic constraint on the components of the vector $\boldsymbol{\theta'} = (\theta_{WG}, \theta_{CS}, \theta_{FS})^T$ and the relation between the torques $\boldsymbol{\tau'} = (\tau_{WG}, \tau_{CS}, \tau_{FS})^T$ are:

$$\begin{cases} \theta_{WG} - (N+1)\theta_{CS} + N\theta_{FS} = 0 \\ \tau_{FS} = -N\tau_{WG} \\ \tau_{FS} = \frac{N}{N+1}\tau_{CS} \end{cases} \tag{2}$$

The dynamical model of the system is:

$$\boldsymbol{B'}\ddot{\boldsymbol{\theta}}' + \boldsymbol{C'}\dot{\boldsymbol{\theta}}' = \boldsymbol{\tau}', \tag{3}$$

where $\boldsymbol{\tau}'$ is the vector of the torques acting on the shafts and

$$\boldsymbol{B'} = \begin{bmatrix} J_{WG} & 0 & 0 \\ 0 & J_{CS} & 0 \\ 0 & 0 & J_{FS} \end{bmatrix} \boldsymbol{C'} = \begin{bmatrix} c_{WG} & 0 & 0 \\ 0 & c_{CS} & 0 \\ 0 & 0 & c_{FS} \end{bmatrix} \tag{4}$$

are the matrices of inertia and viscous damping respectively. The terms $J$ and $c$ indicate the inertia and damping of each shaft. Considering the kinematic constraint in the first equation of (2), the configuration of the system can be expressed in terms of two variables ($\theta_{WG}$ and $\theta_{CS}$). As reported in [20], by introducing the matrix

$$\boldsymbol{R} = \begin{bmatrix} 1 & 0 \\ 0 & 1 \\ -\frac{1}{N} & \frac{N+1}{N} \end{bmatrix} \tag{5}$$

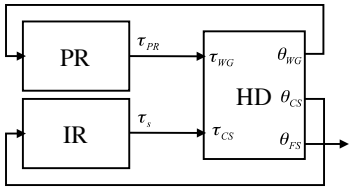


Fig. 4. Block diagram of the VIDA. HD block implements equation (6). The IR block represents the model shown in Fig. 6. $\theta_{FS}$ represents the rotation of the load.

equation (3) becomes:

$$\boldsymbol{B}\ddot{\boldsymbol{\theta}} + \boldsymbol{C}\dot{\boldsymbol{\theta}} = \boldsymbol{\tau} \tag{6}$$

In (6) $\boldsymbol{\theta} = (\theta_{WG}, \theta_{CS})^T = \boldsymbol{R}^T\boldsymbol{\theta}'$ and $\boldsymbol{\tau} = (\tau_{WG}, \tau_{CS})^T = \boldsymbol{R}^T\boldsymbol{\tau}'$ are the vectors of the two independent angular and torque variables respectively; $\boldsymbol{B} = \boldsymbol{R}^T\boldsymbol{B}'\boldsymbol{R}$ and $\boldsymbol{C} = \boldsymbol{R}^T\boldsymbol{C}'\boldsymbol{R}$ are the inertia and viscous damping matrices in the independent coordinates. Considering a load connected to the FS, its moment of inertia $J_L$ can be added to that of the FS in the matrix $\boldsymbol{B}$.

### *B. Actuators model*

Both the PR and the IR are modeled in their mechanical and electrical part, considering the moment of inertia of the rotor $J$, the viscous damping $b$ and the motor inductance and resistance $L$ and $R$. In the case of the PR, which is directly connected to the WG of the Harmonic Drive, the moment of inertia $J_{PR}$ and the viscous damping $b_{PR}$ can be directly added to those of the WG in the matrices $\boldsymbol{B}'$ and $\boldsymbol{C}'$ respectively. In the case of the IR, a typical SEA model (such as the one presented in [19]) is considered. In Fig. 5 a schematization of the model in the Laplace domain is reported; $K_s$ is the spring stiffness, $\tau_{IR}$ is the torque applied to the rotor, $\omega_{IR}$ is the velocity of the motor, $\tau_s$ is the torque applied to the CS, $\theta_{CS}$ is the rotation of the CS, $V_{IR}$ is the voltage command, $k_t$ is the torque constant and $k_e$ is the back-EMF constant.

### *C. System control*

The regulation of the equilibrium position of the output shaft is pursued through a standard high gain position control of the PR. Impedance regulation is achieved by controlling the output torque of the IR. The ideal torque input at the CS shaft is:

$$\tau_{CS} = K_v(\theta_{FS} - \theta_{FS,d}) + c_v(\dot{\theta}_{FS} - \dot{\theta}_{FS,d}) = \\ = \left(\frac{N+1}{N}\right)^2 \left[K_v(\theta_{CS} - \theta_{CS,d}) + c_v(\dot{\theta}_{CS} - \dot{\theta}_{CS,d})\right] \tag{7}$$

By imposing $\theta_{CS,d} = 0$, $\dot{\theta}_{CS,d} = 0$ the visco-elastic behavior of the output shaft is pursued around the current position, which is set by the PR.

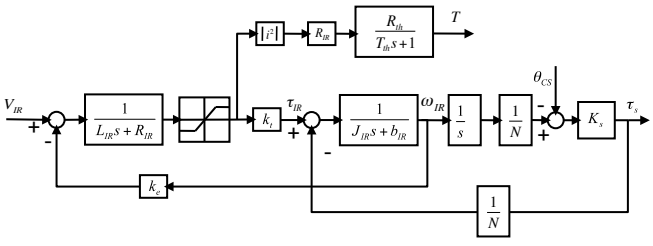


Fig. 5. IR model in Laplace domain. The output torque is $\tau_s = K_s(\frac{\omega_{IR}}{s} - \theta_{CS}) = K_s(\theta_{IR} - \theta_{CS})$. The block with the thermal resistance ($R_{th}$) and the thermal time constant ($T_{th}$) allows to monitor motor winding temperature.

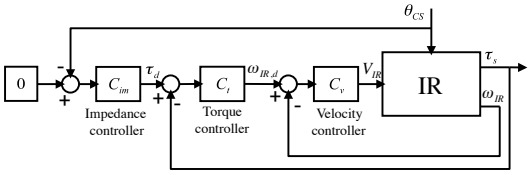


Fig. 6. Block diagram of the IR control. IR block represents the model of Fig. 5. The three cascade controllers implement the transfer functions in (8). By imposing a 0 reference value for the impedance controller, the visco-elastic behavior of the output shaft is every-time pursued around the current output position.

The IR is controlled as proposed in [21]: an inner PI velocity loop is implemented to use the actuator as a velocity sourced (*VS-SEA*) and an external loop is used to control the torque; this regulation is performed by measuring the deflection $\Delta\theta_s$ of the series elastic element (of stiffness $K_s$) and estimating the torque applied to the load $\tau_s$, which is given by the relation $\tau_s = -K_s\Delta\theta_s = K_s(\theta_{IR} - \theta_{CS})$. An outer loop, closed on the load angle measurement, implements the impedance control in the form of (7) in order to render virtual stiffness $K_v$ and damping $c_v$. The three cascade controllers are reported in (8); a block diagram of the control scheme is reported in Fig. 6.

$$\begin{aligned} C_v &= P_v + \tfrac{I_v}{s} \\ C_t &= K_t \tfrac{s^2+as+b}{s^2} \\ C_{im} &= K_v + sc_v \end{aligned} \tag{8}$$

## IV. VALIDATION RESULTS

The model of the VIDA was implemented in Simulink/Matlab (The MathWorks Inc.). The values assigned to the parameters of the model are reported in Table I.

TABLE I
MODEL PARAMETERS

| Parameter | Value |
|---|---|
| $J_{WG}$ | $65 \cdot 10^{-6}$ kg · m$^2$ |
| $J_{CS}$ | $32.9 \cdot 10^{-6}$ kg· m$^2$ |
| $J_{FS}$ | $3.8 \cdot 10^{-2}$ kg· m$^2$ |
| $J_l$ | 5 kg· m$^2$ |
| $b_{WG}$ | $10^{-4}$ N· m· s · rad$^{-1}$ |
| $b_{CS}$ | $8.03 \cdot 10^{-2}$ N· m· s · rad$^{-1}$ |
| $b_{FS}$ | $8.55 \cdot 10^{-2}$ N· m· s · rad$^{-1}$ |
| $N$ | 160 |
| $K_s$ | 200 N· m· rad$^{-1}$ |
| $J_{IR} = J_{PR}$ | $1.35 \cdot 10^{-5}$ kg· m$^2$ |
| $b_{IR} = b_{PR}$ | $2.05 \cdot 10^{-2}$ N· m· s · rad$^{-1}$ |
| $R_{IR} = R_{PR}$ | 0.978 Ω |
| $L_{IR} = L_{PR}$ | 0.573 mH |
| $k_t = k_e$ | $33.5 \cdot 10^{-3}$ V· s · rad$^{-1}$ |
| $R_{th}$ | 8.75 K·W$^{-1}$ |
| $T_{th}$ | 16.6 s |

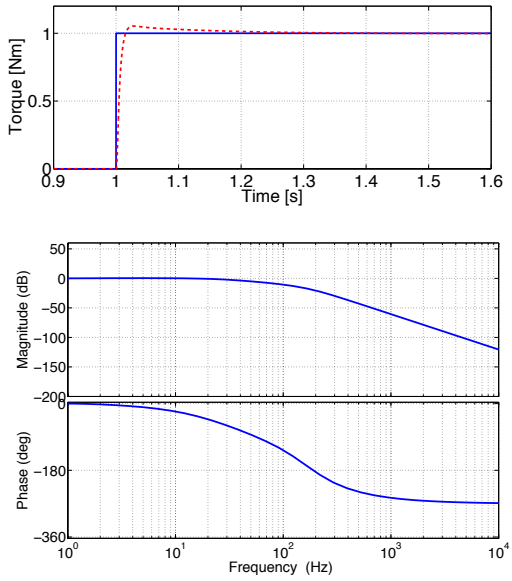


Fig. 7. Step response and Bode diagram of the IR torque control.

### A. Torque control

The step response and the Bode diagram of torque control ($T_s(s)/T_d(s)$) are reported in Fig. 7; a closed loop bandwidth of 35 Hz (at -3 dB) is achieved.

### B. Thermal considerations

Thermal limitations of the IR for three values of the stiffness of the elastic element are reported in Fig. 8. Windings temperature is calculated through a first order transfer function which takes into account the thermal resistance ($R_{th}$) and the thermal time constant ($T_{th}$) (see the block diagram of Fig. 5). Assuming a fixed load ($\theta_{CS} = 0$) the IR was commanded to track sinusoidal torques with frequencies ($f_{tor}$) from 0.1 Hz to 35 Hz; for each frequency the maximal torque amplitude ($A_{tor}$) before overheating (i.e. before motor winding temperature exceeds the maximum allowed temperature for standard thermal exchange conditions) was plotted. It can be seen that a higher stiffness allows to deliver higher torques (up to twice when moving from $K_s$=100 N·m/rad to $K_s$=200 N·m/rad) before the motor overheats.

### C. Impedance regulation

The mechanical output impedance is defined as the amount of torque delivered by an actuator for a given load motion. In our case the output impedance can be defined as $Z_{out}(s) = T_s(s)/\Theta_{CS}(s)$. To test the capability of the VIDA (and in particular of the IR component) to render a virtual impedance, external position perturbations have been simulated. In particular, the output shaft was forced to move sinusoidally with an amplitude of 0.1 rad and a frequency of 1 Hz for different values of $K_v$ and $c_v$ set by the IR. In Fig. 9 the ideal torque (the one obtained multiplying the desired impedance and the imposed external rotation) and the actual torque (the one effectively delivered by the VIDA in response to the external position disturbance) are shown: graphs on the left represent a pure compliant behavior ($c_v$ = 0 N·m·s/rad) while graphs on the right provide the response considering a non-null damping. The desired mechanical impedance can be correctly rendered except for the case of a low pure stiffness. In Fig. 9 the case of $K_v = 10$ N·m/rad is reported; this value is more than one order of magnitude smaller than the stiffness of the physical series elastic element ($K_s = 200$ N·m/rad).

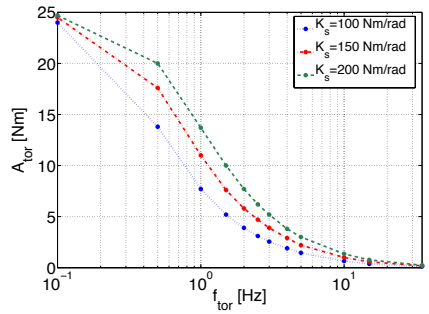


Fig. 8. Thermal limitations of the IR for different series elastic elements ($K_s$ =100, 150 and 200 N·m/rad). IR was commanded to track sinusoidal torque of amplitude $A_{tor}$ and frequency $f_{tor}$ with a fixed load ($\theta_{CS} = 0$).

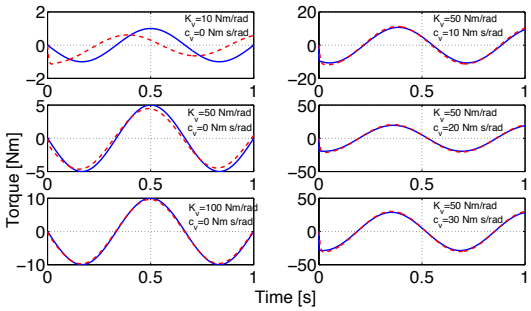


Fig. 9. VIDA torque response to external position perturbations for different virtual impedances (ideal in solid blue, actual in dotted red). A sinusoidal rotation (amplitude 0.1 rad and frequency 1 Hz) was applied on the output.

### D. Positioning tasks

In this section the simulations of positioning tasks, for different rendered virtual impedances, are presented. In Fig. 10 the response of the VIDA to a step command of 20 deg is shown for $K_v = 100$ N·m/rad (top) and $c_v = 40$ N·m·s/rad (bottom). The same positioning task was simulated considering a torque disturbance; at $t = 4$ s, a 5 N·m step torque, simulating the interaction with an external body, was applied on the output shaft. Results are reported in Fig. 11; virtual damping was $c_v = 40$ N·m·s/rad while virtual stiffness was 50 N·m/rad (top) and 20 N·m/rad (bottom).

## V. DISCUSSION AND CONCLUSIONS

In this paper the design of a Variable Impedance Differential Actuator (VIDA) for wearable robotics applications is presented. The model of the system is developed and the expected performances are evaluated through simulations in different conditions. It has been assessed that the VIDA is able to render the desired output impedance when

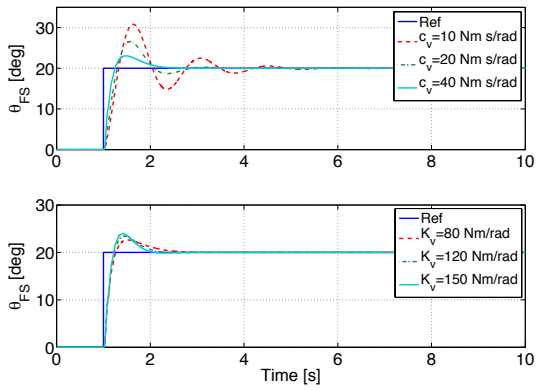


Fig. 10. Response of the VIDA to a step reference position for different values of $K_v$ and $c_v$. $K_v = 100$ N·m/rad (top) and $c_v = 40$ N·m·s/rad (bottom).

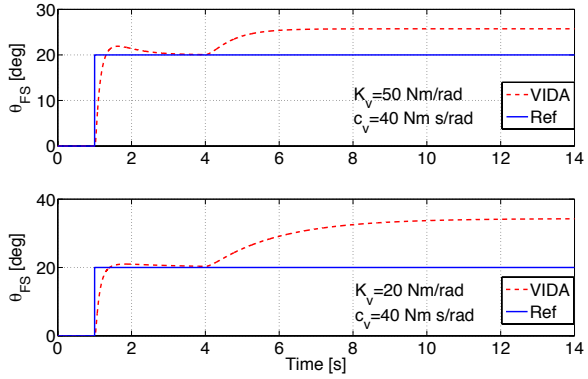


Fig. 11. VIDA positioning task with torque disturbance; at $t = 4$ s, a 5 N·m step torque, simulating the interaction with an external body, is applied on the output shaft. Virtual damping is $c_v = 40$ N·m·s/rad; virtual stiffness is 50 N·m/rad (top) and 20 N·m/rad (bottom).

the requested torque does not exceed the limits of the torque source (i.e. closed loop bandwidth and saturation). Impedance regulation degrades when a pure elastic behavior, with stiffness more than one order of magnitude smaller than the physical spring stiffness, is desired (Fig. 9). It has been verified that the desired impedance can be set while the output equilibrium position is being regulated by the PR (Fig. 10) also when an external torque disturbance is applied (Fig. 11). The presented actuation architecture allows to implement a control strategy where an equilibrium position and impedance field are simultaneously and independently regulated. This is possible still adopting very simple control laws: two separate Single-Input-Single-Output (SISO) controls for position and impedance regulation of the two input shafts.

## VI. ACKNOWLEDGMENTS

This work was supported by the FP7 FET Proactive Initiative "Embodied Intelligence" of the European Commission, project no. ICT-2007.8.5-231451 - EVRYON (EVolving morphologies for human-Robot sYmbiotic interactiON).

## REFERENCES

[1] M. Zinn, O. Khatib, B. Roth, J. K. Salisbury, "Playing it Safe [Human-Friendly Robots]", *IEEE Robotics & Automation Magazine*, vol. 11(2), pp. 12-21, 2004.

[2] A. Albu-Schäffer, O. Eiberger, M. Grebenstein, S. Haddadin, C. Ott, T. Wimböck, S. Wolf, G. Hirzinger, "Soft robotics: From torque feedback controlled light-weight robots to intrinsically compliant systems", *IEEE Robotics and Automation Magazine*, vol. 15(3), 2008, pp. 20–30.

[3] G. A. Pratt and M. M. Williamson, "Series Elastic Actuators", *IEEE/RSJ International Conference on Intelligent Robots and Systems*, Pittsburg, PA, USA, July 1995, pp. 399–406.

[4] J. W. Sensinge, R. F. Weir, "User-Modulated Impedance Control of a Prosthetic elbow in Unconstrained, Perturbed Motion", *IEEE Transactions on biomedical engineering*, vol. 55, 2008, pp. 1043–1055.

[5] N. G. Tsagarakis, M. Laffranchi, B. Vanderborght, D. G. Caldwell, "A compact soft actuator unit for small scale human friendly robots", *IEEE International Conference on Robotics and Automation*, Kobe, Japan, May 2009, pp. 4356–4362.

[6] J. F. Veneman, R. Ekkelenkamp, R. Kruidhof, F. C.T. van der Helm and H. van der Kooij, "A Series Elastic- and Bowden-Cable-Based Actuation System for Use as Torque Actuator in Exoskeleton-Type Robots", *The international journal of robotics research*, vol 25(3), 2006, pp. 261–281.

[7] Y. Mukaibo, S. S. Park, T. Maeno, "Equilibrium Point Control of a Robot Arm with Double Actuation Joint", *International Symposium on Robotics and Automation*, Querétaro, México, August 2004.

[8] B. S. Kim, J. J. Park, J. B. Song, "Double Actuator Unit with Planetary Gear Train for a Safe Manipulator", *International Conference on Robotics and Automation*, Roma, Italy, April 2007, pp. 1146–1151.

[9] R. Van Ham, T. G. Sugar, B. Vanderborght, K. W. Hollander, D. Lefeber, "Compliant actuator designs", *IEEE Robotics & Automation Magazine*, vol. 16(3), pp. 81-94, 2009.

[10] K. Koganezawa, "Mechanical stiffness control for antagonistically driven joints", *IEEE/RSJ International Conference on Intelligent Robots and Systems*, August 2005, pp. 2512–2519.

[11] S. A. Migliore, E. A. Brown, and S. P. DeWeerth, "Biologically inspired joint stiffness control", *IEEE International Conference on Robotics and Automation*, Atlanta, Georgia, April 2005, pp. 4519–4524.

[12] T. Morita, S. Sugano, "Development of 4-DOF Manipulator Using Mechanical Impedance Adjuster", *IEEE International Conference on Robotics and Automation*, April 1996, vol. 4, pp. 2902–2907.

[13] J. Choi, S. Hong, W. Lee, S. Kang, "Variable stiffness joint using leaf springs for robot manipulators", *IEEE International conference on Robotics and Automation*, Kobe, Japan, May 2009, pp. 4363–4368.

[14] R. Van Ham, B. Vanderborght, M. Van Damme, B. Verrelst, D. Lefeber, "MACCEPA: the Actuator with Adaptable Compliance for Dynamic Walking Bipeds", *International Conference on Climbing and Walking Robots and Support Technologies for Mobile Machines*, 2005, pp. 759–766.

[15] S. Wolf, G. Hirzinger, "A New Variable Stiffness Design: Matching Requirements of the Next Robot Generation", *International Conference on Robotics and Automation*, Pasadena, CA, USA, May 2008, pp. 1741–1746.

[16] G. Tonietti, R. Schiavi, A. Bicchi, "Design and Control of a Variable Stiffness Actuator for Safe and Fast Physical Human/Robot Interaction", *IEEE International Conference on Robotics and Automation*, 2005, pp. 528–533.

[17] R. Schiavi, G. Grioli, S. Sen, A. Bicchi, "VSA-II: a Novel Prototype of Variable Stiffness Actuator for Safe and Performing Robots Interacting with Humans", *IEEE International Conference on Robotics and Automation*, Pasadena, CA, USA, May 2008, pp. 2171–2176.

[18] R. Pfeifer, M. Lugarella, F. Iida, "Self-Organization, Embodiment, and Biologically Inspired Robotics", *Science*, vol. 318, pp. 1088–1093, 2007.

[19] D. Robinson, Design and analysis of series elasticity in closed-loop actuator force control. Ph.D. dissertation, MIT, Cambridge (MA), USA, 2000.

[20] L. Lemmer and B. Kiss, "Modeling, Identification, and Control of Harmonic Drives for Mobile Vehicles", *IEEE International Conference on Mechatronics*, Budapest, July 2006, pp. 369–374.

[21] G. Wyeth, "Control Issues for velocity Sourced Series Elastic Actuators", *Australasian Conference on Robotics and Automation*, Auckland, New Zealand, December 2006.